

26 **Abstract**

27 Determining whether a cloud will evolve into a thunderstorm is beneficial for understanding
28 thunderstorm formation and is also important for ensuring the safety of society. However, a clear
29 understanding of the microphysics of clouds in terms of the occurrence of lightning activity has
30 not been attained. Vast field observations and laboratory experiments indicate that graupel, which
31 is rimed ice, is a vital hydrometeor for lightning generation, and is the foundation of riming
32 electrification. In this study, polarimetric radar and lightning observations are used to compare the
33 ice microphysics associated with graupel between 57 isolated thunderstorms and 39 isolated
34 non-thunderstorms, and the differences in radar parameters are quantified. Our results for the
35 occurrence of lightning activity in clouds revealed the following results: 1) the maximum
36 difference in graupel volume at the -10°C isotherm height between thunderstorms and
37 non-thunderstorms reached approximately 7.6 km^3 ; 2) the graupel particles approached spherical
38 shapes with a mean differential reflectivity (Z_{DR}) value of 0.3 dB, which likely indicated that
39 heavily rimed graupel was present; 3) the median values of horizontal reflectivity (Z_{H}) or Z_{DR} at
40 positions where the source initiation and channel of the first lightning flashes were nearly 31 dBZ
41 or 0 dB; and 4) 98.2% of the thunderstorms were equipped with a Z_{DR} column, and the mean
42 depth was $\sim 2.5 \text{ km}$. Our study deepens our understanding of lightning physics and thunderstorm
43 formation.

44 **Short summary**

45 Understanding lightning activity is important for meteorology and atmospheric chemistry.
46 However, the occurrence of lightning activity in clouds is uncertain. In this study, we quantified
47 the difference between isolated thunderstorms and non-thunderstorms. We showed that lightning
48 activity was more likely to occur with more graupel volume and/or riming. A deeper Z_{DR} column
49 was associated with lightning occurrence. This information can aid in a deeper understanding of
50 lightning physics.

51 **Keywords:** thunderstorm; lightning; riming; cloud microphysics

52

53

83 Takahashi et al., 1999; Carey and Rutledge, 2000; Basarab et al., 2015; Stolzenburg et al., 2015;
84 Mattos et al., 2016, 2017; Takahashi et al., 2017, 2019; Hayashi et al., 2021; Zhao et al., 2022).
85 Numerical simulation studies also support the NIC mechanism as the main contributor to charge
86 separation conducive to lightning flash triggering at timescales relevant to storm duration (e.g.,
87 Helsdon et al., 2001; Mansell et al., 2005; Barthe and Pinty, 2007). Therefore, graupel is a vital
88 precipitation particle for riming electrification mechanism.

89 Graupel is rimed precipitation ice. However, the mechanisms for graupel formation vary
90 with cloud type. One pathway to graupel that is very common in warm based clouds worldwide
91 is the development of rain drops in warm rain collision-coalescence processes (e.g., Brahams,
92 1986; Beard, 1992; Herzegh and Jameson, 1992; Bringi et al., 1997; Carey and Rutledge, 2000),
93 followed by lofting of the rain drop in the updraft to subfreezing temperatures (which is
94 frequently observed by polarimetric radar, called the differential reflectivity (Z_{DR}) column), then
95 by drop freezing and finally riming into graupel or small hail. This coalescence-freezing
96 mechanism is often the most important pathway to the first graupel/hail, the first significant
97 electrification and the first lightning flash in warm based clouds (e.g., Brahams, 1986; Beard,
98 1992; Herzegh and Jameson, 1992; Bringi et al., 1997; Smith et al., 1999; Carey and Rutledge,
99 2000; Stolzenburg et al., 2015; Mattos et al., 2017). Another pathway to graupel or small hail
100 production is initiated via the aggregation of ice crystals into snow aggregates, followed by
101 riming of the snow aggregate into graupel and possibly even small hail as the rime density
102 increases (Heymsfield, 1982; Li et al., 2018).

103 It should also be emphasized that the formation of graupel is closely related to not only
104 lightning activity but also the strength of updrafts in clouds, and the latent heat of freezing
105 enhances updrafts, promoting severe storm formation (Rosenfeld, 1999; Zhang et al., 2004;
106 Rosenfeld et al., 2008). More droplets freeze aloft and release more latent heat for nucleation,
107 thereby invigorating convective updrafts and producing lightning, and deep convective clouds
108 form (Rosenfeld, 1999; Zhang et al., 2004; Rosenfeld et al., 2008). Therefore, investigating the
109 ice microphysics associated with graupel is essential for understanding thunderstorm formation.

110 Polarimetric radar is ~~the best~~^{a better} observation system for tracking the specific location
111 and timing of a cloud and inferring the microphysical characteristics within clouds (e.g., Seliga

112 and Bringi, 1976; Zrníc and Ryzhkov, 1999; Kumjian, 2013; Hu et al., 2019; Huang et al., 2023).
113 Many studies (e.g., Laksen and Stansbury, 1974; Marshall and Radhakant, 1978; Dye et al., 1986;
114 Vincent et al., 2003; Latham et al., 2007; Woodard et al., 2012; Mattos et al., 2016, 2017;
115 Hayashi et al., 2021; Zhao et al., 2022) have investigated the relationship between ice
116 microphysics and lightning activity and provided methods for predicting the first lightning flash
117 occurrence based on the riming electrification mechanism; specifically, graupel-related
118 reflectivity at -10°C or colder is a commonly supported leading reflectivity parameter for
119 forecasting the first lightning flash (e.g., Laksen and Stansbury, 1974; Marshall and Radhakant,
120 1978; Vincent et al., 2003; Woodard et al., 2012; Hayashi et al., 2021). However, the
121 performances of these methods vary with season, geography, or other atmospheric variables;
122 more directly, different ice microphysics within different clouds dominate. There is no doubt that
123 the graupel signatures inferred by polarimetric radar are universally present in convective clouds,
124 whereas some clouds involve no lightning (e.g., Woodard et al., 2012; Hayashi et al., 2021; Cui
125 et al., 2022; Zhao et al., 2022). Specifically, the graupel signature inferred by the polarimetric
126 radar needs to be partitioned into more details according to the radar parameters. Therefore, we
127 conducted this study to better understand the ice microphysics associated with graupel within
128 thunderstorms.

129 We accomplished this goal by comparing the ice microphysics associated with graupel
130 between isolated thunderstorms and non-thunderstorms during the warm season over southern
131 China and quantifying differences in graupel magnitude and shape (implying the riming
132 efficiency) in radar parameters, instead of studying the evolution variation within the same
133 thunderstorm (the role of some polarimetric signatures would be covered in the same cloud
134 evolution). Furthermore, we discussed the possible microphysics associated with the source
135 initiation and channel of the first lightning flash via 3D lightning mapping. To our knowledge, no
136 other study addressing this topic has been published. In addition, we explored the role of the
137 coalescence-freezing mechanism in the production of lightning based on the information
138 provided by the Z_{DR} column, a narrow vertical extension of positive Z_{DR} values above the 0°C
139 isothermal height associated with updrafts and supercooled liquid water in deep moist convective
140 storms (e.g., Hall et al., 1980; Ryzhkov et al., 1994; Kumjian and Ryzhkov, 2008; Kumjian, 2013;

141 Kumjian et al., 2014; Snyder et al., 2015; Zhao et al., 2020; Chen et al., 2023). Isolated
142 thunderstorms are common in southern China during the warm season (Mai and Du, 2022). From
143 the perspective of isolated storms in the warm season, the physical processes within clouds are
144 easier to explain, and the characteristics of graupel microphysics can be compared with those of
145 cold-based clouds (Li et al., 2018).

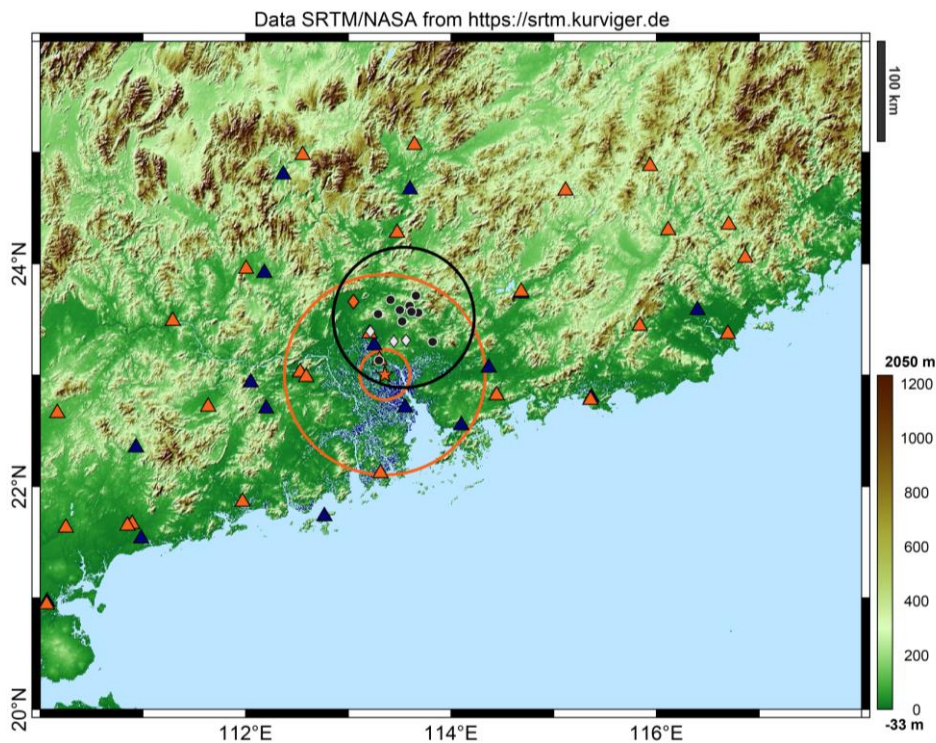
146 **2. Materials and methods**

147 The dataset used in this study was the same as that used in Zhao et al. (2021a, 2022). In Zhao
148 et al. (2021a), the dataset was first shown to the public, ~~who~~ **They** obtained observations of 57 (39)
149 isolated thunderstorms (non-thunderstorms) that occurred over South China in the warm season
150 (from late May to early September) of 2016 and 2017 from the S-band polarimetric radar and
151 three independent lightning location systems. The role of turbulence characteristics in producing
152 the first lightning flashes was evaluated on the basis of the dataset, and the results indicated that
153 the eddy dissipation rate of non-thunderstorms was clearly lower than that of thunderstorms (Zhao
154 et al., 2021a). Moreover, the polarimetric radar parameters of the first radar echoes (the first radar
155 volume scan when clouds are detected by radar) were compared to determine the early difference
156 between thunderstorms and non-thunderstorms on the basis of this dataset (Zhao et al., 2022). The
157 greater echo intensity occurred in non-thunderstorms below the -10°C isotherm height, and the
158 cause for this feature and effect on subsequent cloud development were simply discussed by
159 integrating comprehensive observations (e.g., the ERA-Interim reanalysis data, surface aerosol
160 concentration, and graupel and rainwater contents derived from radar observations).

161 The error in the graupel content estimated in Zhao et al. (2022) is uncertain, and the
162 efficiency of the microphysical process (i.e., riming) associated with graupel is unknown; this
163 represents a gap in understanding ~~regarding~~ the role of graupel in the first lightning flash
164 occurrence based on field observations. Naturally, we aimed to identify a method to quantify
165 differences in graupel magnitude and riming efficiency in this study to minimize the error as much
166 as possible. The radar sample volume, which corresponds to graupel identification, was used to
167 indicate the graupel magnitude instead of the derived graupel content, as in Carey and Rutledge
168 (2000) and Zhao et al. (2022). The variety of Z_{DR} shapes was used to determine the riming
169 efficiency. Thus, the goal and method of this study were substantially different from those of the

170 two previous studies noted above, although they are based on the same dataset.

171 The Guangzhou S-band polarimetric radar (GZ radar) provided the radar data as marked by
172 the orange star in Figure 1. The beam width of the GZ radar was $\leq 1^\circ$, and a full radar volume scan
173 lasted 6 minutes; this consisted of nine elevation angles with a radial resolution of 250 m. A
174 quality control procedure was carried out to remove ground clutter, anomalous propagation, and
175 biological scatter, and the Z_{DR} offset of the raw data was corrected (Zhao et al., 2022). The
176 quality-controlled radar data were interpolated onto a Cartesian grid at a horizontal resolution of
177 250 m and a vertical resolution of 500 m from 0.5 to 20 km above the mean sea level via nearest
178 neighbour and vertical linear interpolation.



179

180 **Figure 1. The locations of the detection systems and the analysed area.** The orange star indicates
181 the Guangzhou S-band polarimetric radar (GZ radar); the orange circles represent distances from the
182 GZ radar site of 25 and 100 km. The black dots indicate the 10 sensors of the Low-Frequency E-field
183 Detection array (LFEDA); the black circle indicates the distance of 70 km from the centre of the
184 LFEDA network to 70 km. The blue triangles indicate the 16 sensors of the Earth Networks Lightning
185 Location System (ENLLS), and the orange triangles indicate the 27 sensors of the Guangdong
186 Lightning Location System (GDLLS). The white diamonds indicate the three ground sites of aerosol
187 concentration measurements. The orange diamond indicates the Qingyuan meteorological observatory.
188 The analysed area is restricted to the regions of overlapping coverage between the GZ radar radius of
189 25–100 km and the LFEDA station network centre radius of 70 km.

190 A hydrometeor identification method, which is based on the fuzzy logic algorithm, was
191 carried out to discriminate the graupel particles, as in Zhao et al. (2021b). The algorithm and
192 approximate ranges of the S-band values of each polarimetric variable essentially followed Park et
193 al. (2009) and Kumjian (2013), with an improvement in the parameters of the membership
194 functions of the fuzzy logic algorithm for the performance of the GZ radar, especially for dry/wet
195 snow particles (Wu et al., 2018). In addition, temperature information was one of the few factors
196 added to the hydrometeor identification method because it can separate liquid precipitation from
197 solid hydrometeors to avoid visible identification errors (e.g., Bechini and Chandrasekar, 2015;
198 Kouketsu et al., 2015; Zhao et al., 2020).

199 Three independent lightning location systems provided lightning observations. The
200 low-frequency E-field detection array (LFEDA, as marked by black dots in Figure 1) can detect
201 three-dimensional structures of intracloud lightning and/or cloud-to-ground lightning. The
202 detection efficiency and mean location error of LFEDA for triggered lightning were approximately
203 100% and 102 m, respectively (Shi et al., 2017; Fan et al., 2018). The Earth Networks Lightning
204 Location System (ENLLS, as marked by blue triangles in Figure 1) can detect two-dimensional
205 locations for intracloud lightning and/or cloud-to-ground lightning. The detection efficiency and
206 mean location error of ENLLS for triggered lightning and the natural strike of tall structure
207 lightning were approximately 77% and 685 m, respectively (Zheng et al., 2017). The Guangdong
208 Lightning Location System (GDLLS, as marked by orange triangles in Figure 1) can locate
209 cloud-to-ground lightning. The detection efficiency and mean location error of the GDLLS for
210 triggered lightning and the natural strike of tall structure lightning were approximately 94% and
211 741 m, respectively (Chen et al., 2012).

212 The lightning flash was assigned to its corresponding cell by using the boundary of the cell as
213 a constraint every 6 minutes. The first lightning flash of a thunderstorm was defined by its first
214 detection from one of three lightning location systems. An isolated non-thunderstorm cell was
215 selected when no flash in the cell was detected by any of the three lightning location systems. To
216 ensure detection-data quality, the analysis area was restricted to the regions of overlapping
217 coverage between the GZ radar radius of 25–100 km and the LFEDA station network centre radius
218 of 70 km (Figure 1), as in Zhao et al. (2021a, 2022). Any isolated cell storm generated within the

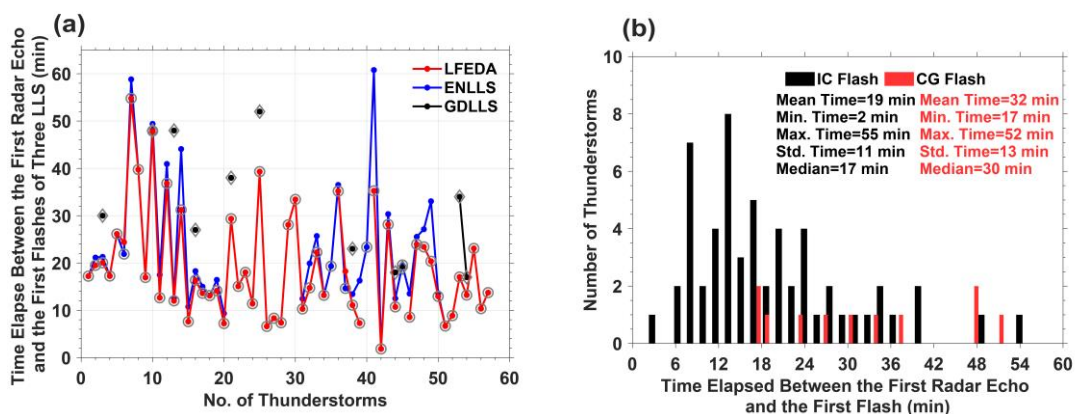
219 analysis area that moved completely outside the analysis area or merged with other precipitation
220 cells was excluded. The intersection of the 20 dBZ contours of the two intersecting cells is
221 referred to as merging. For thunderstorms, we ensure that the first lightning flash of the cell must
222 occur before merging or when there is no merging. For storm cell development, if no merging
223 process occurs and the maximum reflectivity of this cell starts to fade with a value of less than 30
224 dBZ later, the evolutionary process of a cell will mark the cessation stage. Our objective was to
225 focus on isolated storm cells; therefore, if the merging process occurs before the fading of the
226 maximum reflectivity of this cell, the evolutionary process of the cell will also signal the cessation
227 stage.

228 In the dataset, six merging events occurred in non-thunderstorms, and the values of maximum
229 reflectivity for these non-thunderstorms did not increase after merging occurred. In addition, the
230 maximum reflectivity within any non-thunderstorm cell from initiation to cessation must exceed
231 45 dBZ to avoid the statistics of weak precipitation cells. Non-thunderstorms are characterized by
232 no flash occurrence from initiation to cessation. The sounding data were obtained from the
233 Qingyuan meteorological observatory, as marked by the orange diamond in Figure 1, which also
234 provided the environmental temperature. Isolated thunderstorm/non-thunderstorm cells were
235 identified and tracked manually based on the observations from the GZ radar and lightning
236 location systems. The average distances between these storms and the radar/sounding site were
237 approximately 70 and 56 km, respectively. More details related to these data and the selection
238 methods for isolated thunderstorm and non-thunderstorm cells are available in Zhao et al. (2021a,
239 2022).

240 In this study, the evolution cycle of a thunderstorm consists of three stages: (i) the first radar
241 volume scanning in cases where the horizontal reflectivity (Z_H) ≥ 5 dBZ is called the first stage
242 (hereafter referred to as the #1 stage), (ii) the intermediate radar volume scanning between the first
243 stage and the third stage is called the second stage (hereafter referred to as the #2 stage), and (iii)
244 the radar volume scanning in cases where the first lightning flash occurs is called the third stage
245 (hereafter referred to as the #3 stage). Similarly, the evolution cycle of a non-thunderstorm also
246 contains three stages, but radar volume scanning in cases where the most intense echo occurs is
247 called the third stage; here, the most intense echo is used to indicate the strongest convection

248 development stage of non-thunderstorms for comparison with the first lightning flash stage of
 249 thunderstorms. The average durations from the first stage to the third stage for thunderstorms and
 250 non-thunderstorms were 19 and 24 minutes, respectively.

251 The majority of first lightning flash events (~98%) were considered intracloud flashes (IC
 252 flashes), and only one was considered a cloud-to-ground flash (CG flash) (Figure 2a). The
 253 majority of first lightning flashes (~91%) was determined by the LFEDA because of its superior
 254 detection efficiency and accuracy for detecting lightning flashes in this analysis area (Figure 2a).
 255 The elapsed time between the first radar volume scan and the first IC or CG flash (indicated by the
 256 first IC or CG return stroke) is shown in Figure 2b. The results show that the average elapsed time
 257 between the first radar volume scan and the first IC flash was approximately 19 minutes, and the
 258 first CG flash was approximately 32 minutes (Figure 2b). A recent study (Mattos et al., 2017) also
 259 revealed that in ~98% of thunderstorms, the first IC flash preceded the first CG flash, and the IC
 260 flashes occurred approximately 29 minutes after the first radar echo ~~(any reflectivity value (any~~
 261 ~~value above the local noise floor of the radar) at any height)~~, CG flashes were most frequently
 262 delayed by approximately 36 minutes. The definition of the first radar echo may be the possible
 263 reason that the first flashes occurring after the first radar echo in Mattos et al. (2017) occurred
 264 later than those in our study.



265
 266 **Figure 2. Lightning observations.** Elapsed time between the first radar volume scan and (a) the first
 267 flashes of three lightning location systems, LFEDA (red line), ENLLS (blue line), and GDLLS (black
 268 line), where the grey circles indicate the first IC flashes, the grey diamonds indicate the first CG flashes,
 269 and (b) the elapsed time between the first radar volume scan and the first flashes of thunderstorms, the
 270 first IC flashes (black columns), and the first CG flashes (red columns).

271 In addition, the average 1-hourly surface concentration observations of particulate matter

272 (PM_{2.5/10}) were provided by three ground sites (Figure 1, white diamonds) within the analysed area.
273 The PM_{2.5/10} concentration data suggest that the environment prior to these isolated thunderstorms
274 or non-thunderstorms was clean and that the difference in the environmental aerosol concentration
275 between thunderstorms and non-thunderstorms may be small (the mean values of PM_{2.5/10}
276 concentrations prior to thunderstorms and non-thunderstorms were 22.9/42 $\mu\text{g m}^{-3}$ and 20.5/38.8
277 $\mu\text{g m}^{-3}$, respectively).

278 **3. Results**

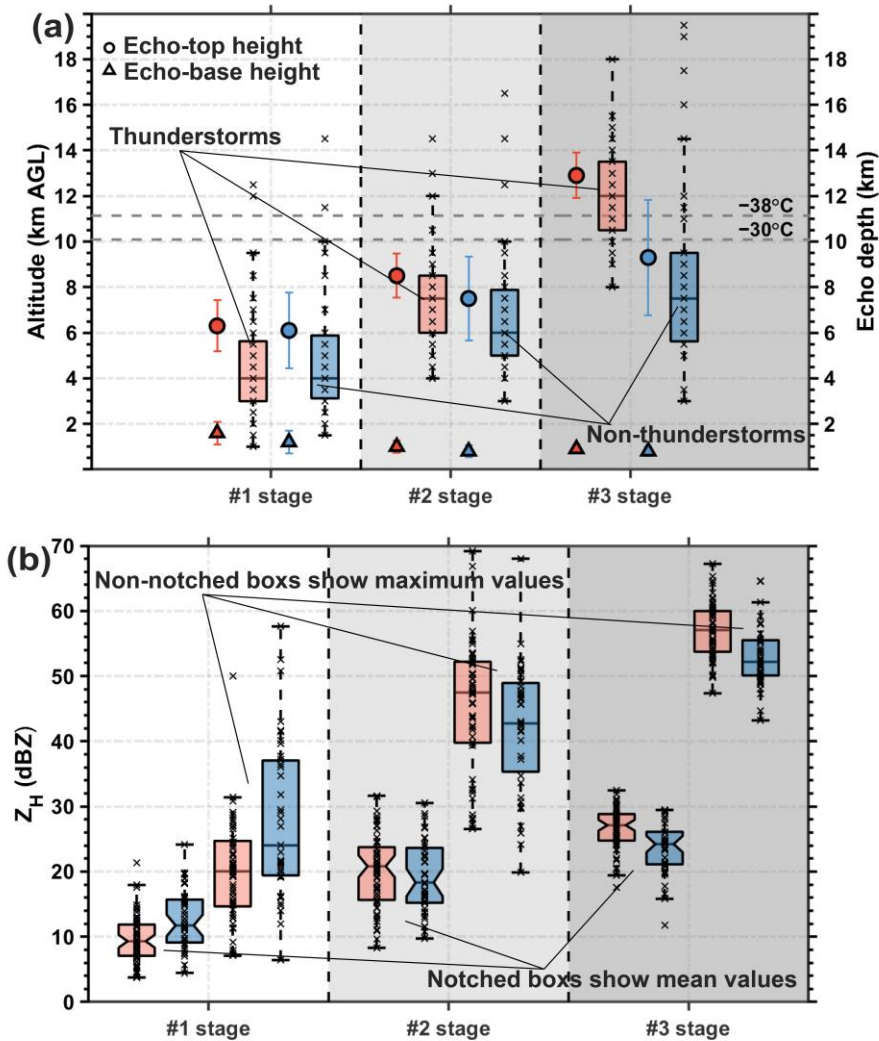
279 **3.1 Morphology and intensity of the echoes in and/or before the first lightning flash** 280 **occurrence**

281 The scatters and triangles with error bars in Figure 3a depict the echo-top heights and
282 echo-base heights of the 57 thunderstorms and 39 non-thunderstorms from the first stage to the
283 third stage of cloud development via the reflectivity threshold (0 dBZ), and the echo depths are
284 shown in the box plots. The echo-top heights of thunderstorms and non-thunderstorms increase as
285 clouds develop. For the echo-top height data, approximately 95% of the thunderstorms exceeded
286 the -30°C isotherm height, and 85% exceeded the -38°C isotherm height of the glaciated layer
287 during the third stage of cloud development; however, only 26% and 23% of the
288 non-thunderstorms exceeded the -30°C and the -38°C isotherm heights, respectively, during the
289 third stage of cloud development. However, the echo-base heights mildly decreased with the
290 development of clouds; slight differences in the echo-base heights occurred between
291 thunderstorms and non-thunderstorms.

292 When the first lightning flashes occurred, approximately 84% of the thunderstorms and only
293 23% of the non-thunderstorms achieved an echo depth of 10 km. Lightning is the product of the
294 severe storms, and scientists often equate storm intensity with lightning flashes (e.g., Zipser et al.,
295 2006; Fan et al., 2018), but defining convective intensity is not as easy as it may seem (Zipser et
296 al., 2006); this could provide supplementary quantitative evidence for assisting scientists in
297 equating storm intensity with lightning flashes and determining the cloud depth corresponding to
298 the first lightning flash occurrence.

299 Figure 3b shows that the differences in the mean (maximum) values of the Z_H between the

300 thunderstorm and non-thunderstorm periods during each stage are slight; specifically, the median
 301 differences in the mean values are -2 , 2 , and 3 dBZ, respectively. The median differences in the
 302 maximum values are -4 , 5 , and 5 dBZ, respectively. Thunderstorms exhibit greater Z_H intensities
 303 than non-thunderstorms do, except for those in the first stage of cloud development. The signature
 304 of larger mean or maximum values of Z_H in non-thunderstorms during the first stage than in
 305 thunderstorms has been discussed by Zhao et al. (2022), and this aspect is not the focus of this
 306 study. The mean or maximum values of Z_H in thunderstorms increase and exceed those in
 307 non-thunderstorms when the first lightning flashes occur; however, the box plots show that we
 308 cannot effectively differentiate thunderstorms from non-thunderstorms with respect to the Z_H
 309 intensity.



310

311 **Figure 3. Characteristics of radar echoes with cloud development.** (a) Echo-top heights of 0 dBZ

312 and echo-base heights of 0 dBZ for 57 thunderstorm and 39 non-thunderstorm cells from the first stage
313 to the third stage of cloud development are indicated by scatter points and triangles, respectively, with
314 error bars. Error bars are computed as 95% confidence intervals. Box plots for the 57 thunderstorms
315 (orange) and 39 non-thunderstorms (blue) for echo depths; all units are in km. The dashed grey lines
316 indicate the -38°C and -30°C isotherm heights. (b) The mean (maximum) value of the Z_{H} in a
317 thunderstorm or a non-thunderstorm during every stage is shown in notched box plots (non-notched
318 box plots), with all units in the dBZ. The median values in the box plots are shown as black horizontal
319 continuous lines. The temperature data were obtained from the sounding data of the Qingyuan
320 meteorological observatory.

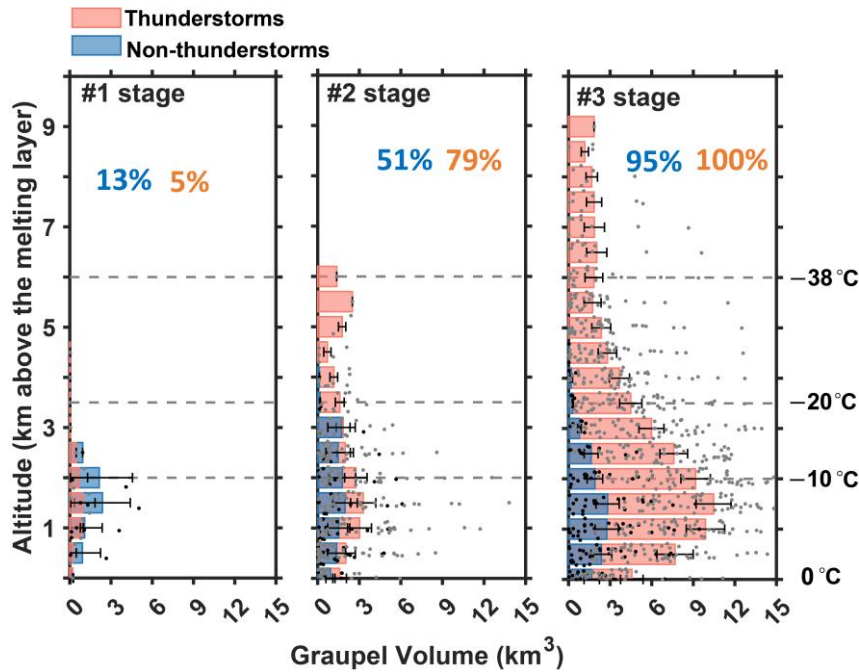
321 **3.2 Variations in graupel magnitude with cloud development**

322 Graupel is a vital precipitation particle for the riming electrification mechanism, and its radar
323 signature is not obscured by small ice particles. Thus, to investigate the microphysical
324 characteristics related to the first lightning flash occurrence during storms, we obtained inferred
325 “graupel”, which was derived from the fuzzy-logic method based on the GZ radar (Park et al.,
326 2009; Kumjian, 2013; Zhao et al., 2021b, 2022).

327 Each bar in Figure 4 indicates the mean value of the graupel volume in a height layer (the
328 definition of the height layer is a vertical resolution of 500 m over 0.5 to 20 km above the mean
329 sea level, 40 height layers in total) for 57 thunderstorms or 39 non-thunderstorms during each
330 stage of cloud development. Specifically, the volume is computed by accumulating the radar
331 sample grids; each radar sample grid is 0.03125 km^3 , $0.25 \text{ km} \times 0.25 \text{ km} \times 0.5 \text{ km}$.

332 Graupel is rare in thunderstorms or non-thunderstorms during the first stage of cloud
333 development (e.g., Dye et al., 1986; Mattos et al., 2017), and only 5% (13%) of thunderstorms
334 (non-thunderstorms) show graupel signals (Figure 4). This finding is consistent with the results of
335 Lang and Rutledge (2011), who indicated that the existence of a 30 dBZ echo above the freezing
336 altitude is a necessary condition (in $\sim 90\%$ of cases) for lightning occurrence. This value is well
337 above the 5 dBZ threshold used in this study to detect the first stage of a storm and can explain
338 why graupel is rare in this stage. Moreover, in a modelling study of an isolated thunderstorm,
339 Barthe and Pinty (2007) reported a delay of ~ 20 minutes between the first occurrence of graupel
340 and the first lightning flash. In this case study, this delay was attributed to the time for graupel and
341 vapour-grown ice to locally gain charge through the NIC mechanism and to the sedimentation of
342 the different particles leading to macroscopic charge separation.

343 We proposed a mechanism for explaining the larger graupel volume in non-thunderstorms
 344 during the first stage of cloud development: more warm precipitation growth in non-thunderstorms
 345 due to cyclic drop growth resulting from coalescence under weaker updrafts may promote greater
 346 drop formation (Kumjian et al., 2014; Mather et al., 1986; Stough et al., 2021). These larger drops
 347 are lifted above the 0°C isothermal height and freeze to graupel-sized particles via a
 348 coalescence-freezing mechanism (e.g., Bringi et al., 1997; Carey and Rutledge, 2000). With the
 349 development of clouds, that proportion of thunderstorms (non-thunderstorms) that produced
 350 graupel reaches 79% (51%) and 100% (95%) during the second and third stages of cloud
 351 development, respectively.



352

353 **Figure 4. Distribution of graupel signals and volume with cloud development.** Histogram plots
 354 with error bars for the distribution of the graupel volume above the melting layer for thunderstorm and
 355 non-thunderstorm cells during each stage of cloud development. Each grey dot indicates the total
 356 graupel volume on a height layer (the definition of the height layer is a vertical resolution of 500 m
 357 over 0.5 to 20 km above the mean sea level, 40 height layers in total) of a thunderstorm; the black dots
 358 indicate non-thunderstorms (units in km³). The mean graupel volume in a height layer for the 57
 359 thunderstorms is displayed as an orange histogram and a blue histogram shows the graupel volume for
 360 non-thunderstorm (in km³). Error bars are computed as 95% confidence intervals. The numerical values
 361 in orange and blue are the percentages of thunderstorms and non-thunderstorms that show graupel
 362 signals, respectively. The left column represents the first stage of cloud development, and the right and
 363 middle rows represent the third and second stages of cloud development, respectively. The -10°C,
 364 -20°C, and -38°C isotherm heights are displayed in the histogram plots.

365 The greatest difference in graupel magnitude between thunderstorms and non-thunderstorms
366 is found during the third stage of cloud development; the maximum difference in graupel volume
367 in a height layer reaches approximately 7.6 km^3 , and the height of the maximum difference is near
368 the -10°C isotherm height. This information is consistent with the NIC electrification mechanism;
369 namely, more graupel leads to more cloud electrification. In addition, more graupel corresponds to
370 more latent heat being released for convection invigoration. Interestingly, that the height
371 corresponding to maximum difference of graupel volume is consistent with the main negative
372 charge layer in thunderstorms over Guangzhou (Liu et al., 2020). Thus, the results suggested that
373 the location of the negative charge layer may depend on the height of the maximum graupel
374 magnitude. Notably, the graupel volume should be more accurately phrased as the presence of
375 graupel in this volume. These characteristics indicate that graupel signals are universally present in
376 thunderstorms and non-thunderstorms and that the difference in the magnitude of the graupel
377 volume is the key for the first lightning flash occurrence.

378 **3.3 More microphysical information based on radar variables**

379 As the graupel volume increases from the first radar track to the occurrence of the first
380 lightning flash, the graupel volume in thunderstorms is clearly greater than that in
381 non-thunderstorms during the third stage of cloud development. However, the understanding of
382 the details of the increase in graupel volume is limited (e.g., the variation in the maximum
383 dimension or number concentration and precursor signature). In addition, although the
384 coalescence-freezing mechanism dominating the formation of graupel within warm-season
385 thunderstorms is generally accepted (e.g., Brahams, 1986; Beard, 1992; Herzegh and Jameson,
386 1992; Bringi et al., 1997; Smith et al., 1999; Carey and Rutledge, 2000; Stolzenburg et al., 2015;
387 Mattos et al., 2017), more studies are needed to support this mechanism.

388 The Z_{DR} parameter could provide more information on graupel (e.g., shape) (e.g., Mattos et
389 al., 2017; Li et al., 2018) and supercooled liquid water (e.g., Z_{DR} column) (e.g., Kumjian, 2013;
390 Kumjian et al., 2014). The variance in the shape of the graupel indicates the riming efficiency;
391 specifically, the heavily rimed ice particles approach a spherical shape (Kumjian, 2013; Li et al.,
392 2018). Although the shape cannot directly indicate the variation in the maximum dimension, the
393 speculated riming efficiency from the variation in the graupel shape could provide related

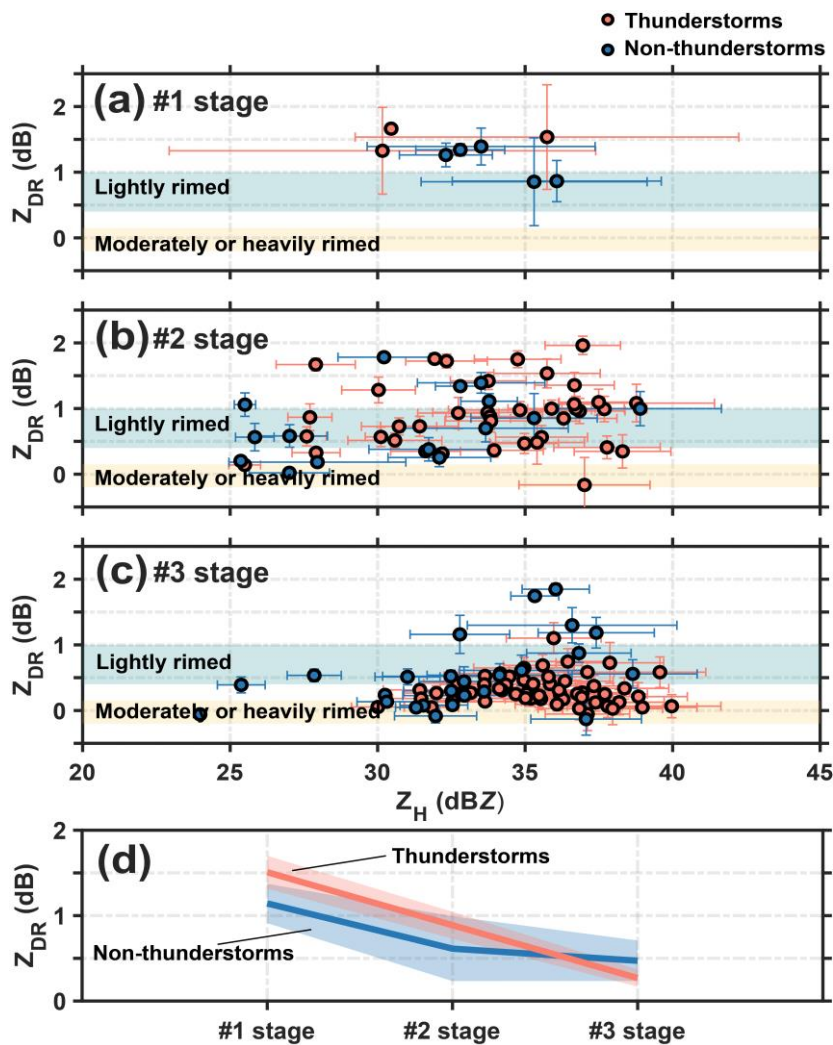
394 information on the maximum dimension of graupel particles; typically, a more spherical shape (a
395 decrease in Z_{DR}) and more riming result in a stronger Z_H corresponding to a larger maximum
396 dimension (Li et al., 2018). The supercooled liquid water indicated by positive Z_{DR} values above
397 the 0°C isothermal height is the precursor for freezing particles, followed by the embryo of
398 graupel particles (e.g., Carey and Rutledge, 2000). Thus, the existence and/or variance of the Z_{DR}
399 column before the occurrence of the first lighting flash could support the coalescence-freezing
400 mechanism. Moreover, we can obtain the quantitative difference in the Z_{DR} between thunderstorms
401 and non-thunderstorms, especially for the occurrence of the first lightning flash.

402 *a. Differences in the shapes of graupel particles between thunderstorms and non-thunderstorms*

403 The mean values of Z_H and Z_{DR} corresponding to graupel particles (the radar sample grids are
404 identified as graupel) above the $\sim -3^\circ\text{C}$ isotherm height (avoiding melting effects) in
405 thunderstorms and non-thunderstorms during each stage of cloud development are displayed in
406 Figure 5. Each orange dot indicates the mean values of Z_H and Z_{DR} corresponding to graupel
407 above the $\sim -3^\circ\text{C}$ isotherm height in a thunderstorm; each blue dot indicates that in a
408 non-thunderstorm. On the basis of these results, the average intensity of the Z_{DR} corresponding to
409 the graupel particles decreases with cloud development, which indicates that the graupel particles
410 gradually approach a spherical shape (Figure 5d). The most remarkable indicator is that the
411 graupel particles in the majority of the thunderstorms have lower Z_{DR} values with a mean value of
412 ~ 0.3 dB when the first lightning flashes occur; however, this lower Z_{DR} value is not evident in
413 non-thunderstorms, even during the most intense echo stage of cloud development, with a mean
414 value of ~ 0.5 dB. Moreover, the Z_{DR} values approach 0 dB, corresponding to stronger Z_H values
415 when the average intensity of the Z_H exceeds 35 dBZ. Thus, we speculated that heavily rimed
416 graupel was present, the size increased, and the shape tended to be spherical.

417 Li et al. (2018) presented a quantitative relationship between the riming and shape of snow
418 aggregates in only winter snowstorms; however, we examined the relationship in deep convection
419 or thunderstorms in the present study. In Li et al. (2018), particles with $Z_H > 15$ dBZ, $Z_{DR} > 0.4$ dB,
420 and above the $\sim -3^\circ\text{C}$ isotherm height are likely to be lightly rimed (rime mass fraction $\sim < 0.2$),
421 and particles with $Z_H > 15$ dBZ, $-0.2 < Z_{DR} < 0.15$ dB, and above the $\sim -3^\circ\text{C}$ isotherm height are
422 likely to be moderately or heavily rimed (rime mass fraction $\sim > 0.4$). The rime mass fraction is

423 defined as the ratio of the accreted ice mass to the total ice particle mass; more details on the rime
 424 mass fraction can be found in Li et al. (2018). In Figures 5a, b, and c, the shaded area in blue
 425 indicates the high possibility that graupel particles are lightly rimed; in contrast, the shaded area in
 426 yellow indicates that the graupel particles are moderately or heavily rimed, as in Li et al. (2018).
 427 The results from Li et al. (2018) are limited to only winter snowstorms; the mechanism for
 428 producing graupel in winter snowstorms is initiated via the aggregation of ice crystals into snow
 429 aggregates, followed by riming of the snow aggregate into graupel and possibly even small hail as
 430 the rime density increases (Heymsfield, 1982; Li et al., 2018). This process is different from the
 431 coalescence-freezing mechanism in warm-season thunderstorms, but the final shape of the graupel
 432 particles when first lightning flashes occurred in this study approached the shape of moderately or
 433 heavily rimed ice particles in Li et al. (2018).



434

435 **Figure 5. Graupel shape in and/or before the first lightning flash occurrence.** Scatter plots with
 436 error bars for the mean values of Z_H and Z_{DR} corresponding to graupel particles above the ~-3°C

437 isotherm height in thunderstorm (orange) and non-thunderstorm (blue) cells during each stage of cloud
438 development. Error bars are computed as 95% confidence intervals. The inferred differences in the
439 efficiency of the riming process are shown by the threshold values of Z_H and Z_{DR} ; the shaded area in
440 blue indicates the high possibility that graupel particles are lightly rimed, and comparatively, the
441 shaded area in yellow indicates that graupel particles are moderately or heavily rimed. (a) First stage, (b)
442 second stage, and (c) third stage of cloud development. In addition, the statistical mean values are
443 given in (d), and the orange (blue) line indicates the mean value of the Z_{DR} corresponding to the above
444 scatters in thunderstorms (non-thunderstorms) during each stage of cloud development. The shaded
445 area indicates the 95% confidence interval.

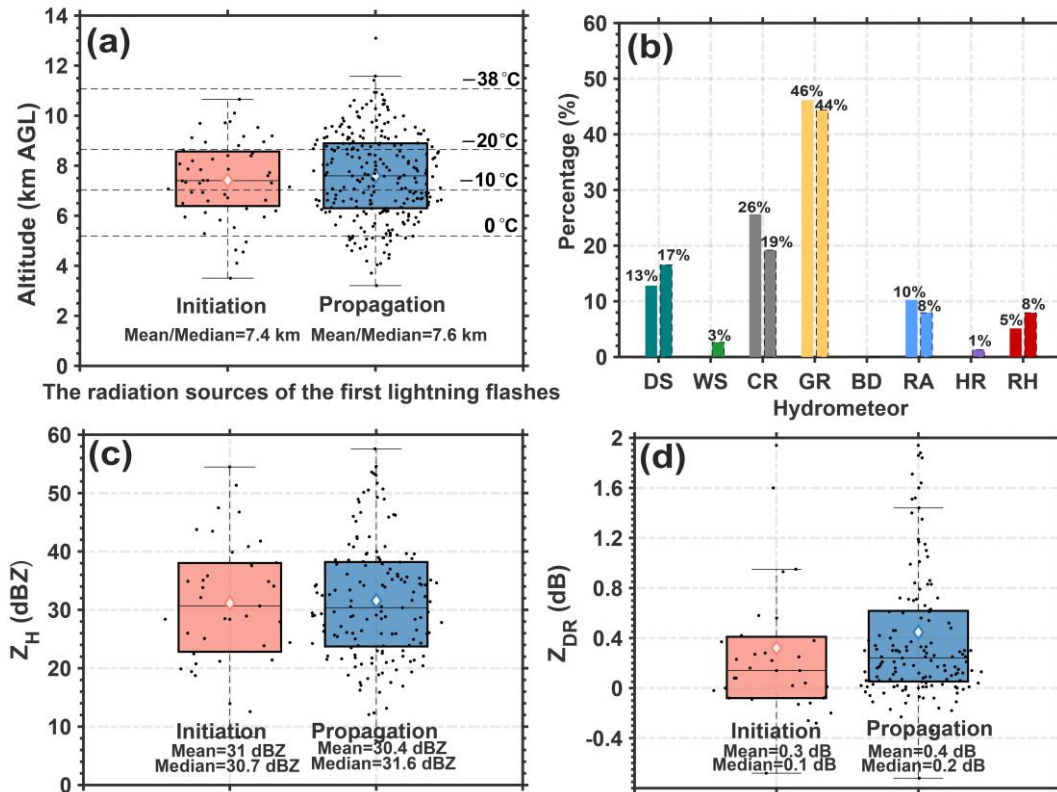
446 *b. Observational characteristics associated with the source initiation and channel of the first*
447 *lightning flash*

448 The characteristics at positions with source initiation and channel characteristics of the first
449 lightning flash are shown in Figure 6, including the height distribution, associated hydrometeor
450 type, and values of Z_H and Z_{DR} . The heights of the initiation sources and propagation sources of
451 the first lightning flashes determined via LFEDA are concentrated at an approximate -10°C
452 isotherm height (Figure 6a), which is consistent with the results (i.e., the negative charge layer is
453 located at 6 to 8 km height in thunderstorms over Guangzhou) reported by Liu et al. (2020). The
454 hydrometeor types associated with the initiation and propagation sources are similar, and the
455 majority of these particles are graupel and ice crystals (Figure 6b), which is understandable on the
456 basis of the NIC electrification mechanism.

457 The median values of Z_H are near 31 dBZ, and the Z_{DR} values are near 0 dB (Figure 6c, d).
458 Furthermore, Figure 7 displays the frequency of initiation and propagation sources corresponding
459 to value intervals of Z_H (4 dBZ) and Z_{DR} (0.2 dB). The results indicate that the initiation sources of
460 the first lightning flashes likely correspond to 20~40 dBZ and $-0.2\sim 0.4$ dB (Figure 7a), and the
461 values are likely 16~44 dBZ and $-0.2\sim 0.8$ dB from propagation sources, respectively (Figure 7b).

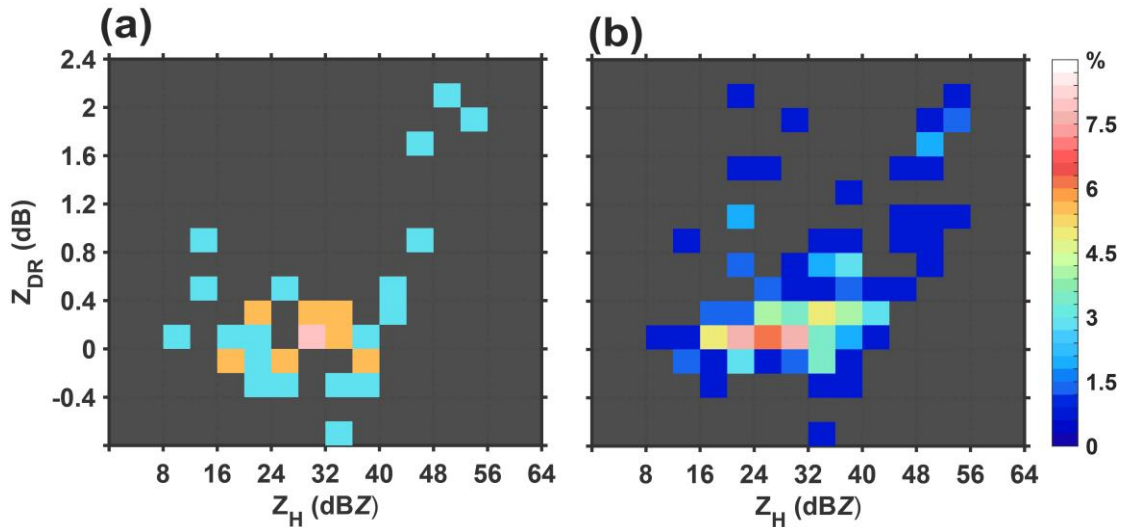
462 ~~These characteristics~~ The heights of the initiation sources and propagation sources of the first
463 lightning flashes within isolated thunderstorms over Guangzhou are concentrated at an
464 approximate -10°C isotherm height, which provides supplementary evidence that the main
465 negative charge layer is located at -10°C to -20°C isotherm height on Earth, as reported by
466 Krehbiel (1986). ~~and~~ The values of Z_H (Z_{DR}) corresponding to the initiation sources and
467 propagation sources of the first lightning flashes suggest that are differences in particle shape

468 and/or size between initiation sources and propagation sources, although the differences are too
 469 subtle to quantify in this study.



470

471 **Figure 6. The characteristics at positions with source initiation and the channel of the first**
 472 **lightning flash.** (a) Height distribution of the locations at the initial sources (orange box) or
 473 propagation sources (blue box) of the first lightning flashes. The 0°C, -10°C, -20°C, and -38°C
 474 isotherm heights are displayed. (b) The histogram indicates the percentage of various hydrometeors of
 475 the locations at the initial sources or propagation sources (histogram with dashed line) of the first
 476 lightning flashes. The numerical value is the percentage of various hydrometeors, such as dry snow (DS,
 477 dark green), wet snow (WS, green), crystals (CR, grey), graupel (GR, yellow), big drops (BD),
 478 raindrops (RA, blue), heavy rain (HR, purple), and rain and hail mixtures (RH, red). Radar parameters
 479 of the locations at the initial sources (orange box) or propagation sources (blue box) of the first
 480 lightning flashes: (c) horizontal reflectivity (Z_H) and (d) differential reflectivity (Z_{DR}). Each black dot
 481 indicates an individual source. The diamonds indicate the mean values.



482

483 **Figure 7. The frequency of radiation sources corresponding to the value intervals of Z_H and Z_{DR} .**

484

(a) Initial sources. (b) Propagation sources.

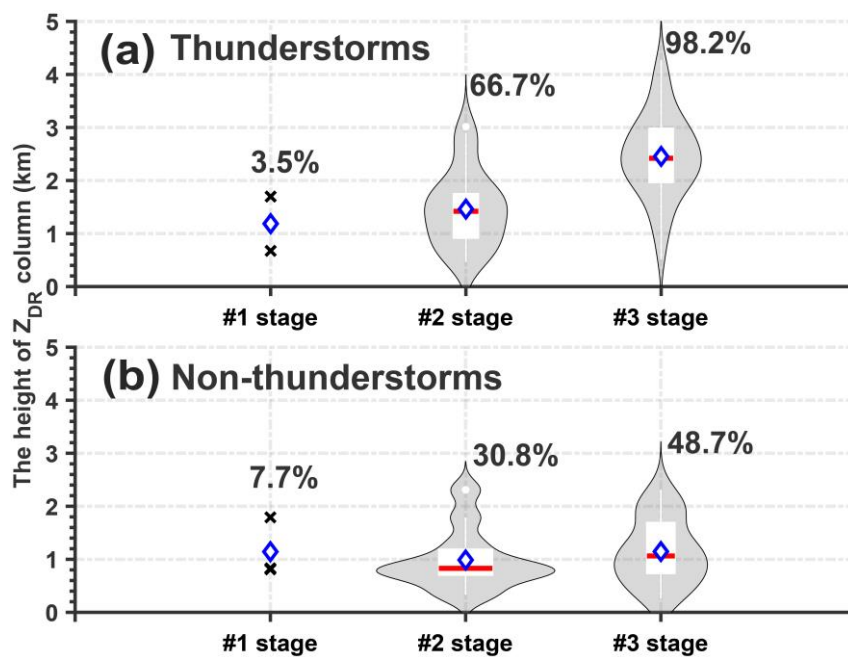
485 *c. Signature of the Z_{DR} column*

486 Previous studies utilized Z_{DR} values ranging from 0.5–5 dB within the strong reflectivity
 487 range (35–50 dBZ) above the melting layer to describe the area of the Z_{DR} column (e.g.,
 488 Illingworth et al., 1987; Tuttle et al., 1989; Ryzhkov et al., 1994; Scharfenberg et al., 2005;
 489 Woodard et al., 2012; Kumjian et al., 2014; Snyder et al., 2015; Zhao et al., 2020). Since the
 490 development of these clouds in this study occurred during the early stage of the full evolution
 491 cycle of thunderstorms, the size of the supercooled liquid water drop would not be large. Thus, we
 492 used Z_{DR} values of 0.5 dB within a reflectivity range of 30 dBZ above the melting layer to
 493 investigate the characteristics of the Z_{DR} column.

494 Figure 8 shows the height of the Z_{DR} column within thunderstorms or non-thunderstorms
 495 during each stage of cloud development. The computation of the Z_{DR} column height is similar to
 496 that in Snyder et al. (2015), and this height is the vertically continuous maximum depth of the Z_{DR}
 497 column. The signature of the Z_{DR} column clearly coincides with the development of clouds
 498 (Figure 8). Most thunderstorms (98.2%) displayed a deep Z_{DR} column with a mean depth of the
 499 Z_{DR} column of ~ 2.5 km when the first lightning flash occurred; however, only 48.7% of
 500 non-thunderstorms corresponded to a shallow Z_{DR} column with a mean value of ~ 1.1 km (Figure
 501 8a, b). Moreover, 66.7% of the thunderstorms presented a deeper Z_{DR} column with a mean value
 502 of ~ 1.5 km during the second stage of cloud development, and 30.8% of the non-thunderstorms

503 presented a shallower Z_{DR} column with a mean value of ~ 0.99 km during the second stage of
 504 cloud development (Figure 8a, b).

505 The results indicate that strong relationship between the Z_{DR} column and the occurrence of
 506 the first lightning flash is persistent. A deeper Z_{DR} column suggests a greater graupel volume.
 507 However, the occurrence frequency of the Z_{DR} column for non-thunderstorms is slightly greater
 508 than that for thunderstorms during the first stage of cloud development (Figure 8a, b). This
 509 phenomenon may be related to the results of Zhao et al. (2022); specifically, the Z_{DR} values below
 510 the -10°C isotherm height of non-thunderstorms were greater than those of thunderstorms within
 511 the first radar echo.



512

513 **Figure 8. Z_{DR} column information in and/or before the first lightning flash occurrence.** Violin
 514 plots of the Z_{DR} column depth of thunderstorm or non-thunderstorm cells during each stage of cloud
 515 development, showing the average (blue diamond), interquartile range (rectangle), 10th and 90th
 516 percentiles (whiskers), and kernel density estimation (gray shading). (a) Thunderstorms. (b)
 517 Non-thunderstorms. The numerical value is the percentage of thunderstorms that show the Z_{DR} column
 518 signature.

519 4. Summary

520 In this study, a combination of a lightning location system and dual-polarization radar
 521 measurements was employed to study the ice microphysics of isolated thunderstorms and
 522 non-thunderstorms in southern China during the warm season. From the unique perspective of

523 comparing radar signatures and inferred graupel information between isolated thunderstorm and
524 non-thunderstorm cells during each stage of cloud development, lightning generation in clouds
525 was found to be a good indicator of the formation of deep convective clouds. The echo intensities,
526 echo-top heights and echo depths were greater in clouds when the first lightning flash occurred,
527 which indicated more severe updrafts in thunderstorms than in non-thunderstorms. Moreover, a
528 greater graupel volume was clearly observed in clouds when the first lightning flash occurred, and
529 the maximum difference in graupel volume in the height layer between thunderstorms and
530 non-thunderstorms reached approximately 7.6 km^3 , corresponding to an approximate -10°C
531 isotherm height.

532 The variation in the average Z_{DR} intensity corresponding to the graupel particles above the
533 $\sim -3^\circ\text{C}$ isotherm height during the three stages of cloud development indicated that graupel
534 particles were more spherical (the mean Z_{DR} value was $\sim 0.3 \text{ dB}$) and were more likely to generate
535 lightning. The Z_{DR} values approached 0 dB , corresponding to stronger Z_{H} values; the average
536 intensity of the Z_{H} exceeded 35 dBZ . When the first lightning flashes occurred in clouds, a
537 decrease in the Z_{DR} value and an increase in the Z_{H} value of graupel were observed; these results
538 indicate that heavily rimed ice particles were present and that the shape of these particles was
539 similar to that of moderately or heavily rimed ice particles within winter snowstorms.

540 Furthermore, observational characteristics associated with the source initiation and channel of
541 the first lightning flash were investigated. The results revealed that these sources were
542 concentrated at an isotherm height of approximately -10°C and mainly corresponded to graupel
543 and ice crystals. The median values of Z_{H} or Z_{DR} at the positions of source initiation and the
544 channel of the first lightning flashes were nearly 31 dBZ or 0 dB . In addition, we suggest that the
545 differences in particle shape and/or size between the initiation sources and propagation sources of
546 the first lightning flashes persist.

547 Moreover, the results indicated a strong relationship between the Z_{DR} column and the
548 occurrence of the first lightning flash; 98.2% of the clouds were equipped with a Z_{DR} column with
549 a mean depth of $\sim 2.5 \text{ km}$ when the first lightning flash occurred. In addition, a deeper Z_{DR} column
550 corresponded to a greater graupel volume. Thus, the coalescence-freezing mechanism dominated
551 the formation of graupel within warm-season isolated thunderstorms over southern China, and the

552 results were consistent with those of previous studies (e.g., Brahams, 1986; Beard, 1992; Herzegh
 553 and Jameson, 1992; Bringi et al., 1997; Smith et al., 1999; Carey and Rutledge, 2000; Stolzenburg
 554 et al., 2015; Mattos et al., 2017) but increased the knowledge of the quantified characteristics of
 555 the Z_{DR} column for the first lightning flash occurrence in warm-season isolated thunderstorms on
 556 the basis of relatively large sample statistics (Table 1 shows details of cases in related
 557 investigations for isolated thunderstorms).

References	Number of cases (thunderstorms)	Number of cases (non-thunderstorms)
Workman and Reynolds, 1949	12	×
Reynolds and Brook, 1956	5	×
Goodman et al., 1988	1	×
Ramachandran et al., 1996	2	×
Jameson et al., 1996	3	×
Woodard et al., 2012	31	19
Stolzenburg et al., 2015	3	×
Mattos et al., 2017	46	×

558 Table 1. Details of the cases in the references.

559 However, our results were obtained by comparing the characteristics of the polarimetric
 560 parameters according to the graupel particles inferred via a hydrometeor identification method.
 561 The inferred graupel volume was an indication that graupel could be present among other
 562 hydrometeors in that volume. From the perspective of radar, the dominant particle in this volume
 563 was graupel. Fortunately, we focused on comparing the graupel volume between thunderstorms
 564 and non-thunderstorms; therefore, we believe that the errors in this volume resulting from other
 565 secondary hydrometeors could be neutralized by comparisons with the same detected data and
 566 methods.

567 In addition, unlike previous similar studies (e.g., Mattos et al., 2016, 2017), we studied the
 568 microphysical differences between isolated thunderstorms and non-thunderstorms during the
 569 warm season over southern China on the basis of polarimetric radar and lightning mapping array
 570 instead of studying the evolution variation within the same thunderstorm (Mattos et al., 2017) or
 571 studying the differences between storm vertical profiles in three-dimensional Cartesian boxes with
 572 lightning and without lightning (Mattos et al., 2016).

573 Although the results from this study could provide a possible index or method based on
574 polarimetric radar for warning of the first lightning flash occurrence within warm-season cell
575 storms, understanding the microphysical characteristics and applying that in the numerical
576 simulations would be the optimal method for providing lightning flash warnings in the future.

577

578

579

580 **Acknowledgements**

581 The authors acknowledge the Guangzhou Institute of Tropical and Marine Meteorology for
582 collecting and archiving the radar, the surface, and the lightning observations. And authors also
583 acknowledge the State Key Laboratory of Severe Weather, Chinese Academy of Meteorological
584 Sciences & Laboratory of Lightning Physics and Protection Engineering for three-dimensional
585 lightning location data. This research has been supported by the National Natural Science
586 Foundation of China (grants 42175090, 42305079, 42305087), the China Postdoctoral Science
587 Foundation (grant 2023M730619), the Scientific Research Fund of Chengdu University of
588 Information Technology (grants KYTZ202213, KYQN202301, KYQN202307), the Scientific
589 Research Fund of CAMS State Key Laboratory of Severe Weather (2021LASW-B02), and Basic
590 Research Fund of CAMS (451490, 2023Z008).

591

592 **Open Research**

593 The sounding data is available at <http://weather.uwyo.edu/upperair/sounding.html>. The data in this
594 study can be obtained from Figshare (Zhao, 2024).

595

596

597 **References**

598 Barthe, C., and Pinty, J.-P.: Simulation of electrified storms with comparison of the charge
599 structure and lightning efficiency, *Journal of Geophysical Research*, 112, D19204,

600 doi:10.1029/2006JD008241, 2007.

601 Basarab, B. M., Rutledge, S. A., and Fuchs, B. R.: An improved lightning flash rate
602 parameterization developed from Colorado DC3 thunderstorm data for use in cloud-resolving
603 chemical transport models, *Journal of Geophysical Research: Atmospheres*, 120, 9481–9499,
604 doi:10.1002/2015JD023470, 2015.

605 Beard, K. V.: Ice initiation in warm-base convective clouds: An assessment of microphysical
606 mechanisms, *Atmospheric Research*, 28, 125–152,
607 [https://doi.org/10.1016/0169-8095\(92\)90024-5](https://doi.org/10.1016/0169-8095(92)90024-5), 1992.

608 Bechini, R., and Chandrasekar, V.: A Semisupervised Robust Hydrometeor Classification Method
609 for Dual-Polarization Radar Applications, *Journal of Atmospheric and Oceanic Technology*,
610 32, 22–47, <https://doi.org/10.1175/JTECH-D-14-00097.1>, 2015.

611 Braham, R. R. Jr.: The cloud physics of weather modification. Part 1: Scientific basis, *WMO*
612 *Bulletin*, 35, 215–221, 1986.

613 Bringi, V. N., Knupp, K., Detwiler, A., Liu, L., Caylor, I. J., and Black, R. A.: Evolution of a
614 Florida Thunderstorm during the Convection and Precipitation/Electrification Experiment:
615 The Case of 9 August 1991, *Monthly Weather Review*, 125, 2131–2160, doi:
616 [https://doi.org/10.1175/1520-0493\(1997\)125<2131:EOAFTD>2.0.CO;2](https://doi.org/10.1175/1520-0493(1997)125<2131:EOAFTD>2.0.CO;2), 1997.

617 Brune, W. H., McFarland, P. J., Bruning, E., Waugh, S., MacGorman, D., Miller, D. O., Jenkins, J.
618 M., Ren, X., Mao, J., and Peischl, J.: Extreme oxidant amounts produced by lightning in
619 storm clouds, *Science*, 372, 711–715, doi: 10.1126/science.abg0492, 2021.

620 Carey, L. D., and Rutledge, S. A.: The Relationship between precipitation and lightning in tropical
621 island convection: A C-Band polarimetric radar study, *Monthly Weather Review*, 128,
622 2687–2710, [https://doi.org/10.1175/1520-0493\(2000\)128<2687:TRBPAL>2.0.CO;2](https://doi.org/10.1175/1520-0493(2000)128<2687:TRBPAL>2.0.CO;2), 2000.

623 Chen, G., Zhao, K., Wen, L., Yang, J., Zheng, Y., Xu, F., Lyu, F., Sun, K., and Sun, L.: Linking
624 ice-phase microphysics to raindrop characteristics in deep convection: A warm-sector
625 extreme rainfall case study in Eastern China, *Earth and Space Science*, 10, e2022EA002697,
626 <https://doi.org/10.1029/2022EA002697>, 2023.

627 Chen, L., Zhang, Y. J., Lyu, W., Zheng, D., Zhang, Y., Chen, S., and Huang, Z.: Performance
628 evaluation for a lightning location system based on observations of artificially triggered
629 lightning and natural lightning flashes, *Journal of Atmospheric and Oceanic Technology*, 29,

630 1835–1844, <https://doi.org/10.1175/JTECH-D-12-00028.1>, 2012.

631 Cui, Y., Zheng, D., Zhang, Y. J., Ruan, Z., Li, F., Yao, W., Meng, Q., and Zhao, C.: Association of
632 lightning occurrence with precipitation cloud column structure at a fixed position,
633 *Atmospheric Research*, 267, 105989, <https://doi.org/10.1016/j.atmosres.2021.105989>, 2022.

634 Dye, J. E., Jones, J. J., Winn, W. P., Cerni, T. A., Gardiner, B., Lamb, D., Pitter, R. L., Hallett, J.,
635 and Saunders, C. P. R.: Early electrification and precipitation development in a small, isolated
636 Montana cumulonimbus, *Journal of Geophysical Research: Atmospheres*, 91, 1231–1247,
637 <https://doi.org/10.1029/JD091iD01p01231>, 1986.

638 Fan, J. W., Rosenfeld, D., Zhang, Y., Giangrande, S. E., Li, Z., Machado, L. A. T., Martin, S. T.,
639 Yang, Y., Wang, J., Artaxo, P., Barbosa, H. M. J., Braga, R. C., Comstock, J. M., Feng, Z.,
640 Gao, W., Gomes, H. B., Mei, F., Pöhlker, C., Pöhlker, M. L., Pöschl, U., and de Souza, R. A.
641 F.: Substantial convection and precipitation enhancements by ultrafine aerosol particles,
642 *Science*, 359, 411–418, DOI: 10.1126/science.aan8461, 2018.

643 Fan, X., Zhang, Y. J., Zheng, D., Zhang, Y., Lyu, W., Liu, H., and Xu, L.: A new method of
644 three-dimensional location for low-frequency electric field detection array, *Journal of*
645 *Geophysical Research: Atmospheres*, 123, 8792–8812,
646 <https://doi.org/10.1029/2017JD028249>, 2018.

647 Goodman, S. J., Buechler, D. E., Wright, P. D., and Rust, W. D.: Lightning and precipitation
648 history of a microburst-producing storm, *Geophysical Research Letters*, 15, 1185–1188,
649 <https://doi.org/10.1029/GL015i011p01185>, 1988.

650 Hall, M. P. M., Cherry, S. M., Goddard, J. W. F., and Kennedy, G. R.: Rain drop sizes and rainfall
651 rate measured by dual-polarization radar, *Nature*, 285, 195–198,
652 <https://doi.org/10.1038/285195a0>, 1980.

653 Hayashi, S., Umehara, A., Nagumo, N., and Ushio, T.: The relationship between lightning flash
654 rate and ice-related volume derived from dual-polarization radar, *Atmospheric Research*, 248,
655 105166, <https://doi.org/10.1016/j.atmosres.2020.105166>, 2021.

656 Helsdon Jr., J. H., Wojcik, W. A. and Farley, R. D.: An examination of thunderstorm-charging
657 mechanisms using a two-dimensional storm electrification model, *Journal of Geophysical*
658 *Research: Atmospheres*, 106(D1), 1165–1192, doi:10.1029/2000JD900532, 2001.

659 Herzegh, P. H., and Jameson, A. R.: Observing Precipitation through Dual-Polarization Radar

660 Measurements, *Bulletin of the American Meteorological Society*, 73, 1365–1376,
661 [https://doi.org/10.1175/1520-0477\(1992\)073<1365:OPTDPR>2.0.CO;2](https://doi.org/10.1175/1520-0477(1992)073<1365:OPTDPR>2.0.CO;2), 1992.

662 Heymsfield, A. J.: A Comparative Study of the Rates of Development of Potential Graupel and
663 Hail Embryos in High Plains Storms, *Journal of the Atmospheric Sciences*, 39, 2867–2897,
664 [https://doi.org/10.1175/1520-0469\(1982\)039<2867:ACSOTR>2.0.CO;2](https://doi.org/10.1175/1520-0469(1982)039<2867:ACSOTR>2.0.CO;2), 1982.

665 Huang, H., Zhao, K., Chan, J. C. L., and Hu, D.: Microphysical Characteristics of
666 Extreme-Rainfall Convection over the Pearl River Delta Region, South China from
667 Polarimetric Radar Data during the Pre-summer Rainy Season, *Advances in Atmospheric*
668 *Sciences*, 40, 874–886, <https://doi.org/10.1007/s00376-022-1319-8>, 2023.

669 Hu, J., Rosenfeld, D., Ryzhkov, A., Zrnic, D., Williams, E., Zhang, P., Snyder, J. C., Zhang, R.,
670 and Weitz, R.: Polarimetric radar convective cell tracking reveals large sensitivity of cloud
671 precipitation and electrification properties to CCN, *Journal of Geophysical Research:*
672 *Atmospheres*, 124, 12194–12205, <https://doi.org/10.1029/2019JD030857>, 2019.

673 Illingworth, A. J., Goddard, J. W. F., and Cherry, S. M.: Polarization radar studies of precipitation
674 development in convective storms, *Quarterly Journal of the Royal Meteorological Society*,
675 113, 469–489, <https://doi.org/10.1002/qj.49711347604>, 1987.

676 Jameson, A. R., Murphy, M. J. and Krider, E. P.: Multiple-parameter radar observations of
677 isolated Florida thunderstorms during the onset of electrification, *Journal of Applied*
678 *Meteorology and Climatology*, 35, 343–354,
679 [https://doi.org/10.1175/1520-0450\(1996\)035<0343:MPROOI>2.0.CO;2](https://doi.org/10.1175/1520-0450(1996)035<0343:MPROOI>2.0.CO;2), 1996.

680 Kouketsu, T., Uyeda, H., Ohigashi, T., Oue, M., Takeuchi, H., Shinoda, T., Tsuboki, K., Kubo, M.,
681 and Muramoto, K.: A Hydrometeor Classification Method for X-Band Polarimetric Radar:
682 Construction and Validation Focusing on Solid Hydrometeors under Moist Environments,
683 *Journal of Atmospheric and Oceanic Technology*, 32, 2052–2074,
684 <https://doi.org/10.1175/JTECH-D-14-00124.1>, 2015.

685 Krehbiel, P. R., Brook, M., and McCrory, R. A.: An Analysis of the Charge Structure of Lightning
686 Discharges to Ground, *Journal of Geophysical Research*, 84, 2432–2456,
687 [doi:10.1029/JC084iC05p02432](https://doi.org/10.1029/JC084iC05p02432), 1979.

688 Kumjian, M. R.: Principles and applications of dual-polarization weather radar. Part I: Description
689 of the polarimetric radar variables, *Journal of Operational Meteorology*, 1, 226–242,

690 doi:10.15191/nwajom.2013.0119, 2013.

691 Kumjian, M. R., Khain, A. P., Benmoshe, N., Ilotoviz, E., Ryzhkov, A. V., and Phillips, V. T. J.:
692 The anatomy and physics of ZDR columns: Investigating a polarimetric radar signature with
693 a spectral bin microphysical model, *Journal of Applied Meteorology and Climatology*, 53,
694 1820–1843, <https://doi.org/10.1175/JAMC-D-13-0354.1>, 2014.

695 Kumjian, M. R., and Ryzhkov, A. V.: Polarimetric signatures in supercell thunderstorms, *Journal*
696 *of Applied Meteorology and Climatology*, 47, 1940–1961,
697 <https://doi.org/10.1175/2007JAMC1874.1>, 2008.

698 Laksen, H. R., and Stansbury, E. J.: Association of lightning flashes with precipitation cores
699 extending to height 7 km, *Journal of Atmospheric and Terrestrial Physics*, 36, 1547–1548,
700 [https://doi.org/10.1016/0021-9169\(74\)90232-3](https://doi.org/10.1016/0021-9169(74)90232-3), 1974.

701 Lang, T. J., and Rutledge, S. A.: A Framework for the Statistical Analysis of Large Radar and
702 Lightning Datasets: Results from STEPS 2000, *Monthly Weather Review*, 139, 2536–2551,
703 <https://doi.org/10.1175/MWR-D-10-05000.1>, 2011.

704 Latham, J.: The electrification of thunderstorms, *Quarterly Journal of the Royal Meteorological*
705 *Society*, 107, 277–298, <https://doi.org/10.1002/qj.49710745202>, 1981.

706 Latham, J., Petersen, W. A., Deierling, W. and Christian, H. J.: Field identification of a unique
707 globally dominant mechanism of thunderstorm electrification, *Quarterly Journal of the Royal*
708 *Meteorological Society*, 133, 1453–1457, <https://doi.org/10.1002/qj.133>, 2007.

709 Li, H., Moisseev, D., and von Lerber, A.: How does riming affect dual-polarization radar
710 observations and snowflake shape? *Journal of Geophysical Research: Atmospheres*, 123,
711 6070–6081, <https://doi.org/10.1029/2017JD028186>, 2018.

712 Liu, Z., Zheng, D., Guo, F., Zhang, Y., Zhang, Y. J., Wu, C., Chen, H., Han, S.: Lightning activity
713 and its associations with cloud structures in a rainstorm dominated by warm precipitation,
714 *Atmospheric Research*, 246, 105120, <https://doi.org/10.1016/j.atmosres.2020.105120>, 2020.

715 Lyu, W., Zheng, D., Zhang, Y., Yao, W., Jiang, R., Yuan, S., Liu, D., Lyu, F., Zhu, B., Lu, G.,
716 Zhang, Q., Tan, Y., Wang, X., Liu, Y., Chen, S., Chen, L., Li, Q., and Zhang, Y. J.: A Review
717 of Atmospheric Electricity Research in China from 2019 to 2022, *Advances in Atmospheric*
718 *Sciences*, 40, 1457–1484, <https://doi.org/10.1007/s00376-023-2280-x>, 2023.

719 MacGorman, D. R., and Rust, W. D.: The electrical nature of storms, *Oxford University Press*, 422

720 pp., 1998.

721 Mai, C., and Du, Y.: Mesoscale moisture transport in determining the location of daytime
722 convection initiations clustered in time and space over southern China, *Journal of*
723 *Geophysical Research: Atmospheres*, 127, e2021JD036098,
724 <https://doi.org/10.1029/2021JD036098>, 2022.

725 Mansell, E. R., MacGorman, D. R., Ziegler, C. L., and Straka, J. M.: Charge structure and
726 lightning sensitivity in a simulated multicell thunderstorm, *Journal of Geophysical Research:*
727 *Atmospheres*, 110, D12101, doi:10.1029/2004JD005287, 2005.

728 Marshall, J. S., and Radhakant, S.: Radar Precipitation Maps as Lightning Indicators, *Journal of*
729 *Applied Meteorology and Climatology*, 17, 206–212,
730 [https://doi.org/10.1175/1520-0450\(1978\)017<0206:RPMALI>2.0.CO;2](https://doi.org/10.1175/1520-0450(1978)017<0206:RPMALI>2.0.CO;2), 1978.

731 Mather, G. K., Morrison, B. J., and Morgan, G. M.: A Preliminary Assessment of the Importance
732 of Coalescence in Convective Clouds of the Eastern Transvaal, *Journal of Applied*
733 *Meteorology and Climatology*, 25, 1780–1784,
734 [https://doi.org/10.1175/1520-0450\(1986\)025<1780:APAOTI>2.0.CO;2](https://doi.org/10.1175/1520-0450(1986)025<1780:APAOTI>2.0.CO;2), 1986.

735 Mattos, E. V., Machado, L. A. T., Williams, E. R., and Albrecht, R. I.: Polarimetric radar
736 characteristics of storms with and without lightning activity, *Journal of Geophysical*
737 *Research: Atmospheres*, 121, 14201–14220, <https://doi.org/10.1002/2016JD025142>, 2016.

738 Mattos, E. V., Machado, L. A. T., Williams, E. R., Goodman, S. J., Blakeslee, R. J., and Bailey, J.
739 C.: Electrification life cycle of incipient thunderstorms, *Journal of Geophysical Research:*
740 *Atmospheres*, 122, 4670–4697, <https://doi.org/10.1002/2016JD025772>, 2017.

741 Park, H. S., Ryzhkov, A. V., Zrnić, D. S., and Kim, K.: The Hydrometeor Classification Algorithm
742 for the Polarimetric WSR-88D: Description and Application to an MCS, *Weather and*
743 *Forecasting*, 24, 730–748, <https://doi.org/10.1175/2008WAF2222205.1>, 2009.

744 Pickering, K. E., Bucsela, E., Allen, D., Ring, A., Holzworth, R., and Krotkov, N.: Estimates of
745 lightning NO_x production based on OMI NO₂ observations over the Gulf of Mexico, *Journal*
746 *of Geophysical Research: Atmospheres*, 121, 8668–8691,
747 <https://doi.org/10.1002/2015JD024179>, 2016.

748 Qie, X., Yuan, S., Chen, Z., Wang, D., Liu D., Sun, M., Sun, Z., Srivastava, A., Zhang, H., Lu, J.,
749 Xiao, H., Bi, Y., Feng, L., Tian, Y., Xu, Y., Jiang, R., Liu, M., Xiao, X., Duan, S., Su, D., Sun,

750 C., Xu, W., Zhang, Y., Lu, G., Zhang, D., Yin, Y., and Yu, Y.: Understanding the
751 dynamical-microphysical-electrical processes associated with severe thunderstorms over the
752 Beijing metropolitan region, *Science China Earth Sciences*, 64, 10–26.
753 <https://doi.org/10.1007/s11430-020-9656-8>, 2021.

754 Ramachandran, R., Detwiler, A., Helsdon, J., Smith, P. L., and Bringi, V. N.: Precipitation
755 development and electrification in Florida thunderstorm cells during Convection and
756 Precipitation/Electrification Project, *Journal of Geophysical Research: Atmospheres*, 101,
757 1599–1619, <https://doi.org/10.1029/95JD02931>, 1996.

758 Reynolds, S. E., and Brook, M.: CORRELATION OF THE INITIAL ELECTRIC FIELD AND
759 THE RADAR ECHO IN THUNDERSTORMS, *Journal of the Atmospheric Sciences*, 13,
760 376–380, [https://doi.org/10.1175/1520-0469\(1956\)013<0376:COTIEF>2.0.CO;2](https://doi.org/10.1175/1520-0469(1956)013<0376:COTIEF>2.0.CO;2), 1956.

761 Reynolds, S. E., Brook, M., and Gourley, M. F.: Thunderstorm charge separation, *Journal of the*
762 *Atmospheric Sciences*, 14, 426–436,
763 [https://doi.org/10.1175/1520-0469\(1957\)014<0426:TCS>2.0.CO;2](https://doi.org/10.1175/1520-0469(1957)014<0426:TCS>2.0.CO;2), 1957.

764 Rosenfeld, D.: TRMM observed first direct evidence of smoke from forest fires inhibiting rainfall,
765 *Geophysical Research Letters*, 26, 3105–3108, <https://doi.org/10.1029/1999GL006066>, 1999.

766 Rosenfeld, D., Lohmann, U., Raga, G. B., O'Dowd, C. D., Kulmala, M., Fuzzi, S., Reissell, A.,
767 and Andreae, M. O.: Flood or drought: How do aerosols affect precipitation? *Science*, 321,
768 1309–1313, doi:10.1126/science.1160606, 2008.

769 Ryzhkov, A. V., Zhuravlyov, V. B., and Rybakova, N. A.: Preliminary results of X-band
770 polarization radar studies of clouds and precipitation, *Journal of Atmospheric and Oceanic*
771 *Technology*, 11, 132–139,
772 [https://doi.org/10.1175/1520-0426\(1994\)011<0132:PROXBP>2.0.CO;2](https://doi.org/10.1175/1520-0426(1994)011<0132:PROXBP>2.0.CO;2), 1994.

773 Saunders, C.: Charge Separation Mechanisms in Clouds, *Space Science Reviews*, 137, 335–353,
774 <https://doi.org/10.1007/s11214-008-9345-0>, 2008.

775 Saunders, C. P. R., Keith, W. D., and Mitzeva, R. P.: The effect of liquid water on thunderstorm
776 charging, *Journal of Geophysical Research*, 96, 11007–11017,
777 <https://doi.org/10.1029/91JD00970>, 1991.

778 Scharfenberg, K. A., Miller, D. J., Schuur, T. J., Schlatter, P. T., Giangrande, S. E., Melnikov, V. M.,
779 Burgess, D. W., Andra, D. L., Foster, M. P. Jr., and Krause, J. M.: The Joint Polarization

780 Experiment: Polarimetric Radar in Forecasting and Warning Decision Making, *Weather and*
781 *Forecasting*, 20, 775–788, <https://doi.org/10.1175/WAF881.1>, 2005.

782 Seliga, T. A., and Bringi, V. N.: Potential Use of Radar Differential Reflectivity Measurements at
783 Orthogonal Polarizations for Measuring Precipitation, *Journal of Applied Meteorology and*
784 *Climatology*, 15, 69–76,
785 [https://doi.org/10.1175/1520-0450\(1976\)015<0069:PUORDR>2.0.CO;2](https://doi.org/10.1175/1520-0450(1976)015<0069:PUORDR>2.0.CO;2), 1976.

786 Shi, D., Zheng, D., Zhang, Y., Zhang, Y. J., Huang, Z., and Lyu, W.: Low-frequency E-field
787 Detection Array (LFEDA)-Construction and preliminary results, *Science China Earth*
788 *Sciences*, 60, 1896–1908, <https://doi.org/10.1007/s11430-016-9093-9>, 2017.

789 Smith, P. L., Musil, D. J., Detwiler, A. G., and Ramachandran, R.: Observations of Mixed-Phase
790 Precipitation within a CaPE Thunderstorm, *Journal of Applied Meteorology and Climatology*,
791 38, 145–155, [https://doi.org/10.1175/1520-0450\(1999\)038<0145:OOMPPW>2.0.CO;2](https://doi.org/10.1175/1520-0450(1999)038<0145:OOMPPW>2.0.CO;2),
792 1999.

793 Snyder, J. C., Ryzhkov, A. V., Kumjian, M. R., Khain, A. P., and Picca, J. C.: A ZDR column
794 detection algorithm to examine convective storm updrafts, *Weather and Forecasting*, 30,
795 1819–1844, <https://doi.org/10.1175/WAF-D-15-0068.1>, 2015.

796 Stolzenburg, M., Marshall, T. C., and Krehbiel, P. R.: Initial electrification to the first lightning
797 flash in New Mexico thunderstorms, *Journal of Geophysical Research: Atmospheres*, 120,
798 11,253–11,276, <https://doi.org/10.1002/2015JD023988>, 2015.

799 Stolzenburg, M., Marshall, T. C., and Rust, W. D.: Serial sounding of electric field through a
800 mesoscale convective system, *Journal of Geophysical Research: Atmospheres*, 106,
801 12371–12380, <https://doi.org/10.1029/2001JD900074>, 2001.

802 Stough, S. M., and Carey, L. D.: Observations of anomalous charge structures in supercell
803 thunderstorms in the Southeastern United States, *Journal of Geophysical Research:*
804 *Atmospheres*, 125, e2020JD033012, <https://doi.org/10.1029/2020JD033012>, 2020.

805 Stough, S. M., Carey, L. D., Schultz, C. J., and Cecil, D. J.: Examining conditions supporting the
806 development of anomalous charge structures in supercell thunderstorms in the Southeastern
807 United States, *Journal of Geophysical Research: Atmospheres*, 126, e2021JD034582,
808 <https://doi.org/10.1029/2021JD034582>, 2021.

809 Takahashi, T.: Riming electrification as a charge generation mechanism in thunderstorms, *Journal*

810 of the Atmospheric Sciences, 35, 1536–1548,
811 [https://doi.org/10.1175/1520-0469\(1978\)035<1536:REAACG>2.0.CO;2](https://doi.org/10.1175/1520-0469(1978)035<1536:REAACG>2.0.CO;2), 1978.

812 Takahashi, T., Tajiri, T., and Sonoi, Y.: Charges on Graupel and Snow Crystals and the Electrical
813 Structure of Winter Thunderstorms, *Journal of the Atmospheric Sciences*, 56, 1561–1578,
814 [https://doi.org/10.1175/1520-0469\(1999\)056<1561:COGASC>2.0.CO;2](https://doi.org/10.1175/1520-0469(1999)056<1561:COGASC>2.0.CO;2), 1999.

815 Takahashi, T., Sugimoto, S., Kawano, T., and Suzuki, K.: Riming Electrification in Hokuriku
816 Winter Clouds and Comparison with Laboratory Observations, *Journal of the Atmospheric*
817 *Sciences*, 74, 431–447, <https://doi.org/10.1175/JAS-D-16-0154.1>, 2017.

818 Takahashi, T., Sugimoto, S., Kawano, T., and Suzuki, K.: Microphysical structure and lightning
819 initiation in Hokuriku winter clouds, *Journal of Geophysical Research: Atmospheres*, 124,
820 13156–13181, <https://doi.org/10.1029/2018JD030227>, 2019.

821 Tuttle, J. D., Bringi, V. N., Orville, H. D., and Kopp, F. J.: Multiparameter radar study of a
822 microburst: Comparison with model results, *Journal of the Atmospheric Sciences*, 46,
823 601–620, [https://doi.org/10.1175/1520-0469\(1989\)046<0601:MRSOAM>2.0.CO;2](https://doi.org/10.1175/1520-0469(1989)046<0601:MRSOAM>2.0.CO;2), 1989.

824 Uman, M. A., and Krider, E. P.: Natural and artificially initiated lightning, *Science*, 246, 457–464,
825 doi:10.1126/science.246.4929.457, 1989.

826 Vincent, B. R., Carey, L. D., Schneider, D., Keeter, K., and Gonski, R.: Using WSR-88D
827 reflectivity data for the prediction of cloud-to-ground lightning: A central North Carolina
828 study, *National Weather Digest*, 27, 35–44, 2003.

829 Woodard, C. J., Carey, L. D., Petersen, W. A., and Roeder, W. P.: Operational utility of
830 dual-polarization variables in lightning initiation forecasting, *Electronic J. Operational*
831 *Meteor.*, 13, 79–102, 2012.

832 Workman, E. J., and Reynolds, S. E.: Electrical activity as related to thunderstorm cell growth,
833 *Bulletin of the American Meteorological Society*, 30, 142–149,
834 <https://doi.org/10.1175/1520-0477-30.4.142>, 1949.

835 Wu, C., Liu, L., Wei, M., Xi, B., and Yu, M.: Statistics-based optimization of the polarimetric
836 radar hydrometeor classification algorithm and its application for a squall line in South China,
837 *Advances in Atmospheric sciences*, 35, 296–316, <https://doi.org/10.1007/s00376-017-6241-0>,
838 2018.

839 Zhang, Y., Lyu, W., Chen, S., Zheng, D., Zhang, Y., Yan, X., Chen, L., Dong, W., Dan, J., and Pan,

840 H.: A review of advances in lightning observations during the past decade in Guangdong,
841 China, *Journal of Meteorological Research*, 30, 800–819,
842 <https://doi.org/10.1007/s13351-016-6928-7>, 2016.

843 Zhang, Y. J., Yan, M., Sun, A., and Guo, F.: Thunderstorm electricity. *China Meteorological Press*,
844 384 pp., 2009.

845 Zhang, Y. J., Sun, A., Yan, M., Guo, F., Qie, X., and Huang, M.: Numerical Simulations of the
846 Effects of Electric Environment on Hail Growth, *Chinese Journal of Geophysics*, 47, 29–37,
847 <https://doi.org/10.1002/cjg2.451>, 2004.

848 Zhao, C.: Data for “On the ice microphysics of isolated thunderstorms and non-thunderstorms in
849 southern China: A radar polarimetric perspective”. Figshare. [Dataset].
850 <https://doi.org/10.6084/m9.figshare.22718437.v6>, 2024.

851 Zhao, C., Zhang, Y. J., Zheng, D., Liu, X., Zhang, Y., Fan, X., Yao, W., and Zhang, W.: Using
852 polarimetric radar observations to characterize first echoes of thunderstorms and
853 nonthunderstorms: A comparative study, *Journal of Geophysical Research: Atmospheres*, 127,
854 e2022JD036671, <https://doi.org/10.1029/2022JD036671>, 2022.

855 Zhao, C., Zhang, Y. J., Zheng, D., Zhou, Y., Xiao, H., and Zhang, X.: An improved hydrometeor
856 identification method for X-band dual-polarization radar and its application for one summer
857 Hailstorm over Northern China, *Atmospheric Research*, 245, 105075,
858 <https://doi.org/10.1016/j.atmosres.2020.105075>, 2020.

859 Zhao, C., Zheng, D., Zhang, Y. J., Liu, X., Zhang, Y., Yao, W., and Zhang, W.: Turbulence
860 Characteristics before the Occurrence of the First Flash in Thunderstorms and
861 Non-Thunderstorms, *Geophysical Research Letters*, 48, e2021GL094821,
862 <https://doi.org/10.1029/2021GL094821>, 2021a.

863 Zhao, C., Zheng, D., Zhang, Y. J., Liu, X., Zhang, Y., Yao, W., and Zhang, W.: Characteristics of
864 cloud microphysics at positions with flash initiations and channels in convection and
865 stratiform areas of two squall lines, *Journal of Tropical Meteorology*, 37, 358–369,
866 doi:10.16032/j.issn.1004-4965.2021.035, 2021b.

867 Zheng, D., Zhang, Y., Zhang, Y., Lyu, W., Chen, L., and Shi, D.: Lightning activity characteristics
868 as indicated by lightning location systems in Guangdong, in: *1st International Workshop of
869 the Southern China Monsoon Rainfall Experiment (SCMREX), Beijing, China, 12–13 April,*

870 2017.

871 Zipser, E. J., Cecil, D. J., Liu, C., Nesbitt, S. W. and Yorty, D. P.: WHERE ARE THE MOST
872 INTENSE THUNDERSTORMS ON EARTH? *Bulletin of the American Meteorological*
873 *Society*, 87, 1057–1072, <https://doi.org/10.1175/BAMS-87-8-1057>, 2006.

874 Zrnich, D. S., and Ryzhkov, A. V.: Polarimetry for Weather Surveillance Radars, *Bulletin of the*
875 *American Meteorological Society*, 80, 389–406,
876 [https://doi.org/10.1175/1520-0477\(1999\)080<0389:PFWSR>2.0.CO;2](https://doi.org/10.1175/1520-0477(1999)080<0389:PFWSR>2.0.CO;2), 1999.

877

878 **Authors contributions**

879 Conceptualization: C. Zhao, Y. Zhang

880 Data curation: C. Zhao, Y. Zhang, D. Zheng, S. Du, and X. Liu

881 Formal analysis: C. Zhao, Y. Zhang, H. Li, X. Peng, P. Zhao, J. Zheng, and J. Shi

882 Funding acquisition: Y. Zhang, C. Zhao

883 Investigation: C. Zhao, Y. Zhang

884 Methodology: C. Zhao, Y. Zhang, and H. Li

885 Project Administration: Y. Zhang

886 Resources: C. Zhao, Y. Zhang

887 Software: C. Zhao, D. Zheng

888 Supervision: Y. Zhang

889 Validation: C. Zhao, Y. Zhang

890 Visualization: C. Zhao, Y. Zhang, and H. Li

891 Writing-original draft: C. Zhao, Y. Zhang, X. Peng, and H. Li

892 **Competing interests**

893 The contact author has declared that none of the authors has any competing interests.